SPANWISE VORTEX STRUCTURE OVER POROUS WALLS IN TURBULENT CHANNEL FLOWS

Kazuhiko Suga

Department of Mechanical Engineering
Osaka Prefecture University
Sakai, Osaka 599-8531, Japan
suga@me.osakafu-u.ac.jp

Yuka Nakagawa

Department of Mechanical Engineering
Osaka Prefecture University
Sakai, Osaka 599-8531, Japan
naka@htlab.me.osakafu-u.ac.jp

Masayuki Kaneda

Department of Mechanical Engineering
Osaka Prefecture University
Sakai, Osaka 599-8531, Japan
mkaneda@me.osakafu-u.ac.jp

ABSTRACT

Spanwise flow field measurements are carried out for turbulent flows in channels with permeable bottom walls by PIV to understand the effects of the wall permeability on turbulence structure near porous walls. The porous media used are three kinds of foamed ceramics which have the same porosities (0.8) but different permeabilities. The turbulent flow fields in spanwise planes are discussed using instantaneous and statistical measurement data. At a small permeability Reynolds number (Re_K), low speed and high speed streaks, which are similar to those of solid-wall turbulence, are observed near the walls while at a large Re_K the observed structure is far different from that of the solid wall turbulence. It is found that the obtained spanwise scales of the structure can be reasonably correlated with the wall normal distance plus the zero-plane displacement which is estimated from the mean velocity profile. With the distribution profiles of the spanwise streak spacing and integral length scales, the transitional change of the turbulence structure over permeable walls is discussed.

INTRODUCTION

Most of the surfaces of real wall materials are not perfectly smooth but have roughness and sometimes permeability as well. Although flow characteristics over permeable surfaces such as foamed metals, woven or non-woven fabrics and vegetative canopies, etc. are different from those over smooth surfaces, it is not fully understood how different they are. Accordingly, to understand the turbulent flow physics over porous media, many people including the authors' group measured turbulent wall flows whose wall surfaces have permeability and analyzed the turbulence statistics and structures, (e.g. Suga *et al.*, 2010, 2011; Suga, 2016). Although the streaky structure looked destroyed by the wall permeability in the DNS (Breugem *et al.*, 2006; Kuwata & Suga, 2016*a*,*b*), according to the authors' knowledge, how the wall permeability influences the turbulence structure has not been well understood. Therefore, the present study attempts to investigate turbulent vortex structure over permeable walls using instantaneous and statistical data by PIV experiments focusing on the wall permeability effects on the spanwise flow structure. Since from our previous studies Suga *et al.* (2010, 2011); Suga (2016), turbulence characteristics were well characterized by the permeability Reynolds number: Re_K and there was a transition to full porous wall turbulence in the range of Re_K=0 – 3, the present study attempts to explicate the change of the spatial structure when the transition occurs.

EXPERIMENTAL METHOD

Fig.1 illustrates the test section of the present experimental setup. Tracer particles are capsules containing Rhodamine B and their mean diameter and specific gravity are respectively 10 μm and 1.50. Tap water is pumped up from a water tank, then the flow is fully developed in a driver channel (3000 mm) and enters the test section. The channel consists of solid smooth acrylic top and side walls and a porous bottom wall. The thickness of the porous wall is about 0.06 m which is twice the clear channel height H=0.03 m of the clear fluid region whose width W is 0.3 m. The porosity of the presently used porous media shown in Fig.2 is φ=0.8 and the permeabilities are K=0.20, 0.33, and $0.87\times10^{-7}\mathrm{m}^2$ for #20, #13 and #06, respectively.

The present planar PIV system consists of a double-pulse Nd-YAG laser with 200 mJ/pulse at a wavelength of 532 nm, two

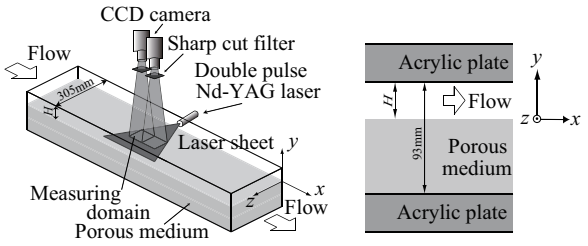

Figure 1. Schematic view of the test section.

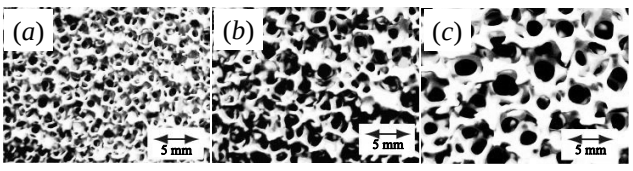

Figure 2. Surface photographs of the foamed ceramics with porosity φ =0.8: (a) #20 ; permeability $K = 0.20 \times 10^{-7}\mathrm{m}^2$, (b) #13 ; $K = 0.33 \times 10^{-7}\mathrm{m}^2$, (c) #06 ; $K = 0.87 \times 10^{-7}\mathrm{m}^2$.

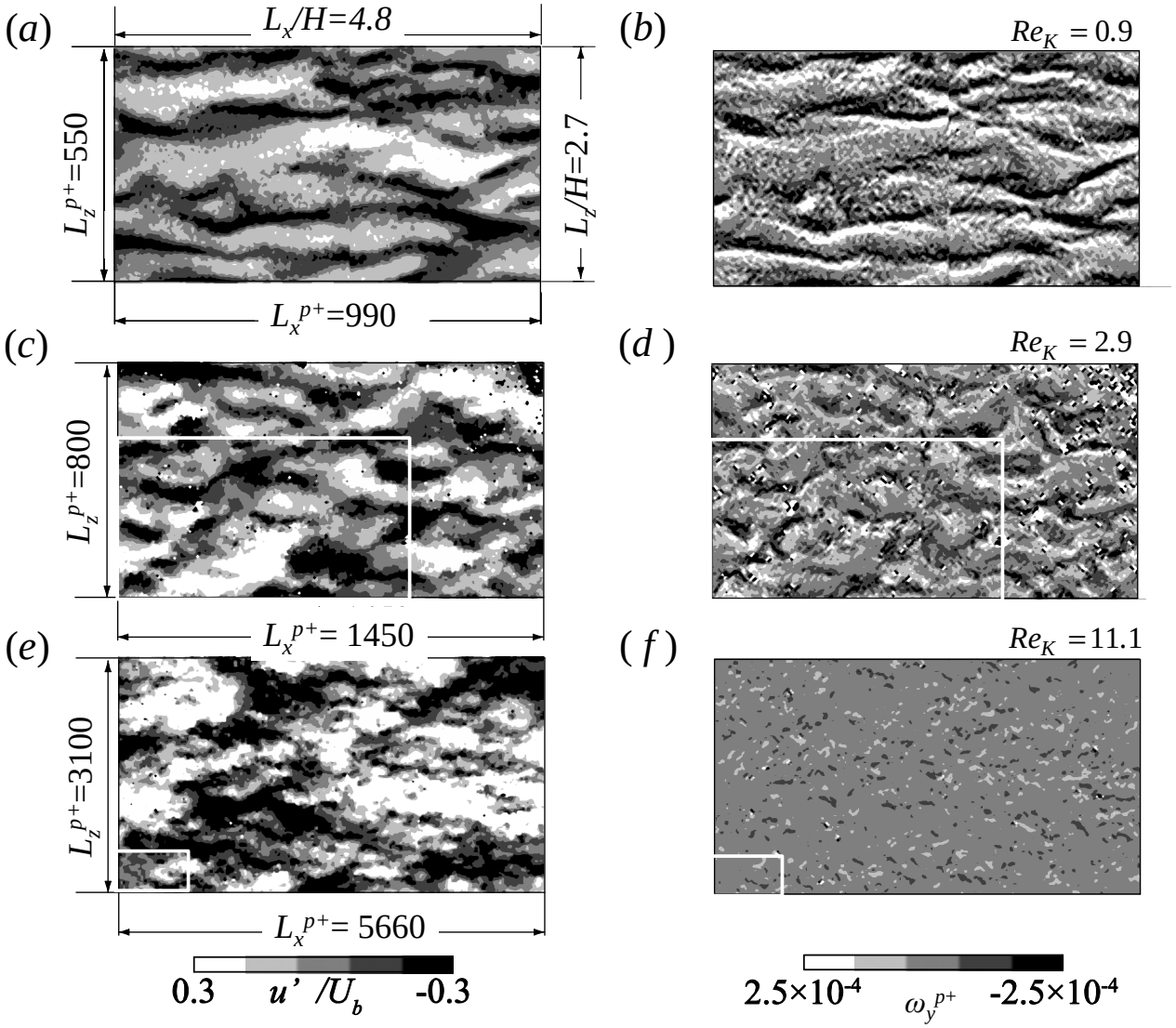

Figure 3. Low and high speed streaks and instantaneous wall normal vorticity ω_y at $y^{p+} \simeq 20$: (a,c,e) are fluctuation velocity contours and (b,d,f) are vorticity contours. (a,b) #20 porous wall at Re_K=0.9, (c,d) #06 porous wall at Re_K=2.9, (e,f) #06 porous wall at Re_K =11.1. The white rectangle areas in (c-f) correspond to the area of (a,b). The flow direction is left to right.

Table 1. Experimental conditions and measured parameters of the mean velocity fields.

wall	s. no.	Re_b	Re_K	u_τ^p/u_τ^t	κ	d^{p+}	h^{p+}
solid	5	5600	-	1.00	-	-	-
#20	5	2500	0.93	1.14	0.40	0	0
	18	5200	1.90	1.23	0.37	7	1
	14*	7200	2.90	1.34	0.29	38	6
	5*	14800	6.23	1.46	0.28	56	17
#13	5	1900	1.07	1.22	-	-	-
	15	3100	1.79	1.34	0.33	11	2
	14	4700	3.00	1.43	0.27	45	12
	5*	10800	6.45	1.54	0.25	76	28
	5*	15900	9.35	1.57	0.28	94	31
#06	15	1500	1.80	1.36	-	-	-
	5*	2700	2.94	1.45	0.32	21	5
	5	3400	3.83	1.52	0.28	26	9
	15	6200	6.73	1.63	0.26	80	27
	5*	9900	11.12	1.70	0.28	123	41

tandemly arranged CCD cameras of 30 fps with lenses of 85 mm f/1.8D and computers for data process. The laser beam is formed into a sheet of approximately 1.0 mm thickness through several cylindrical lenses. The laser sheet illuminates a streamwise-spanwise ($x-z$) plane of the channel where the instantaneous images are recorded by the CCD cameras. A single recorded frame of each camera covers a zone of 80 80 mm^2 with 2048×2048 pixel^2. The number of the particle is adjusted to be about 13 in an interrogation window whose size is set to 32×32 pixel^2. The uncertainty in the measured displacement can be expected to be roughly less than 1/10 of the diameter of the particle image. Normalizing the uncertainty of this mean displacement of particles yields a relative error of less than 4%.

RESULTS AND DISCUSSIONS

The $x-z$ plane measurements are performed for solid smooth wall, #20, #13 and #06 porous wall cases changing Re_b from 1500 to 15900 to achieve the conditions of Re_K roughly at 1.0−11.0. Here, u_τ^p is the friction velocity on the porous wall. There are altogether 15 cases as shown in Table 1. For each case, several measurement planes in the wall normal direction are measured. In Table 1, measured sections 5, 5*, 14, 14*, 15 and 18 correspond to sections (1.0, 2.0, 3.0, 4.0, 5.0 mm), (0.5, 1.0, 1.5, 2.0, 2.5 mm), (1.0, 2.0, 3.0, ⋯ , 14.0, 15.0 mm), (1.0, 2.0, 3.0, ... , 13.0, 14.0 mm), (0.5, 1.0, 1.5, 2.0, 2.5, 3.0, 4.0, ... , 10.0, 11.0 mm) and (0.5, 1.0, 1.5, 2.0, 2.5, 3.0, 4.0, ... , 14.0, 15.0 mm), respectively from the bottom surface. To obtain the bulk mean velocity and the friction velocity by the previously reported method (Suga *et al.*, 2010), $x-y$ plane measurements are also performed for the corresponding cases.

Fig.3 shows images of low and high speed regions over porous walls at $y^{p+}\simeq 20$, where $(\cdot)^{p+}$ is a normalized value by the friction velocity on the porous wall. The existence of the streaky structure is obvious in Fig.3 (a,b) at Re_K=0.9 while they are twisted. In Fig.3 (c,d) at Re_K= 2.9 the twisting degree significantly increases and the streaks are torn in fragments. At the much higher Re_K case of Re_K=11.1 in Fig.3 (f), obviously fragments of streaks no longer exist, however, large scale spanwise patterns seem to be developing as in Fig.3 (e). Indeed, in the streamwise direction black and white block areas can be detected in turn. This is considered to be footprints of the spanwise roles induced by the Kelvin-Helmholtz instability as reported numerically by Kuwata & Suga (2016*a*,*b*) and Jiménez *et al.* (2001).

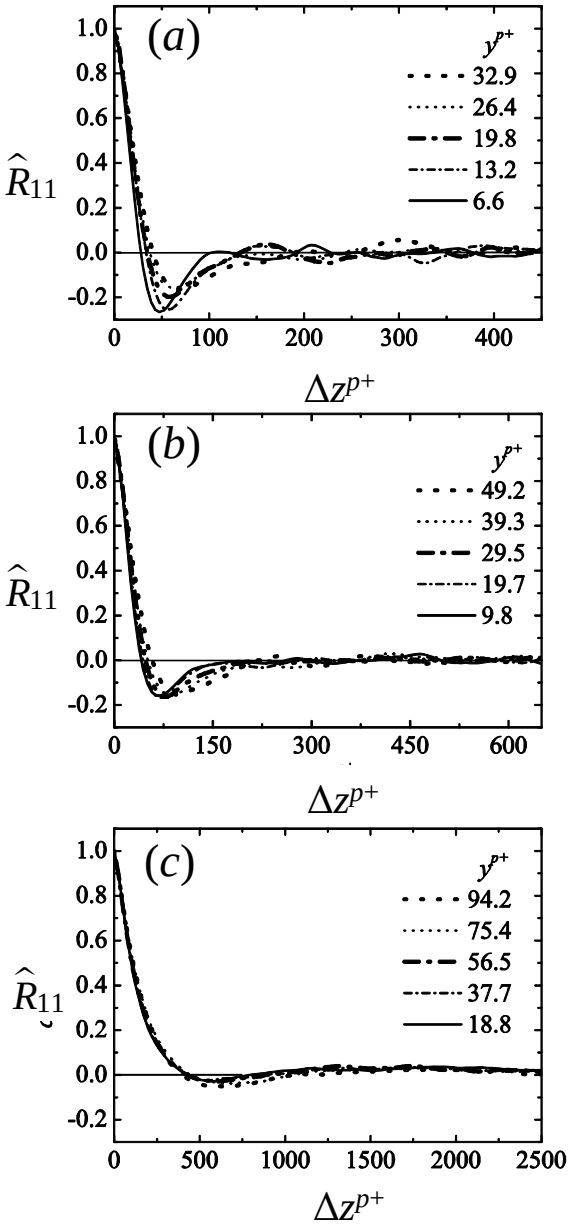

Figure 4. Two-point correlation of the streamwise velocity versus spanwise spacing: (a) #20 at Re_K= 0.9, (b) #13 at Re_K =3.0, (c) #06 at Re_K = 11.1.

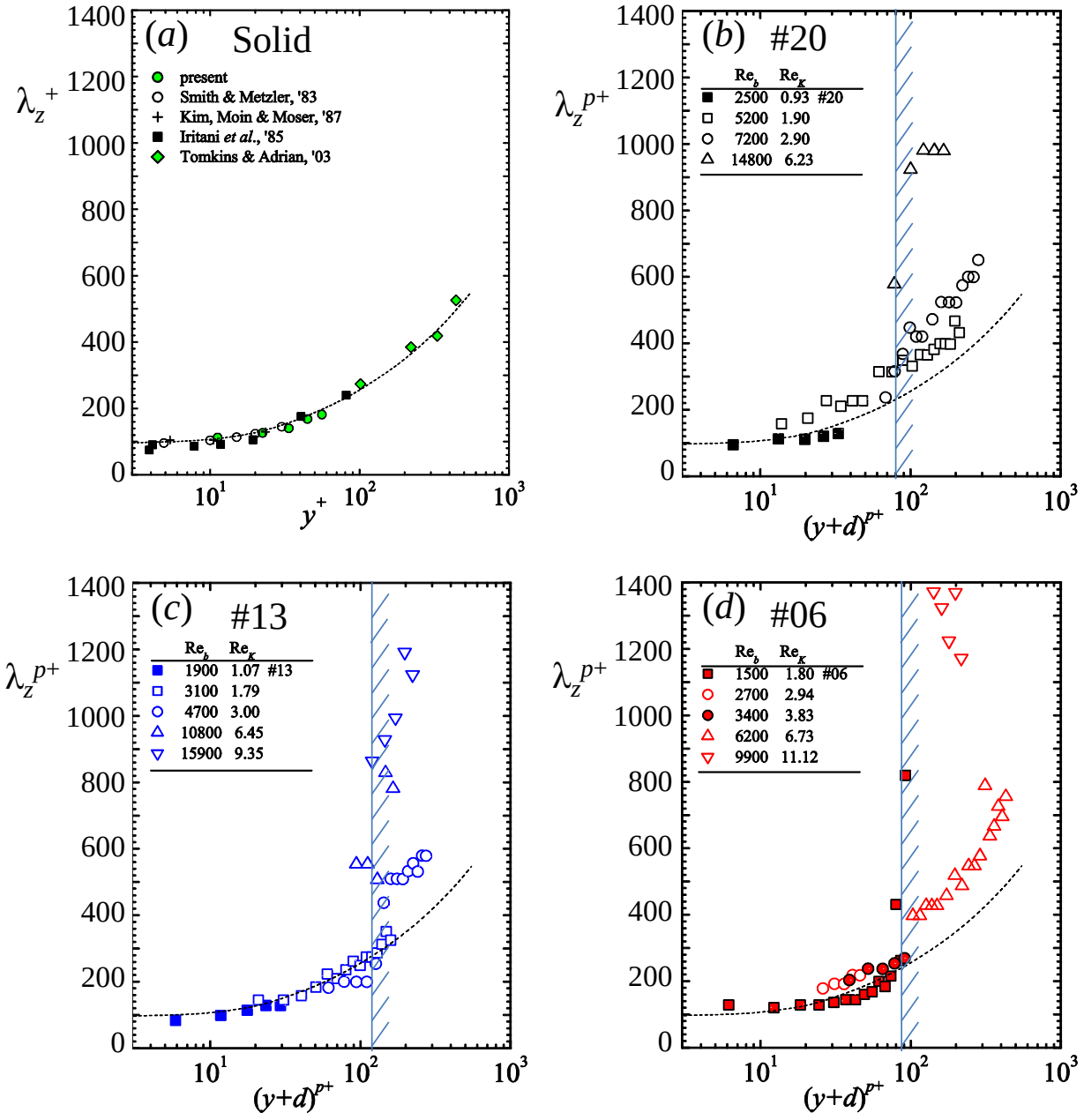

Figure 5. Spanwise spacing of streaks in the wall normal direction: (a) solid smooth wall cases, (b) #20 porous wall cases, (c) #13 porous wall cases, (d) #06 porous wall cases.

As far as the structure scale is concerned, it is obvious that as Re_K increases the field scale normalized by the inner scale increases. Note that the normalized area corresponding to those of Fig.3(a) and (b) are indicated with the white rectangles in Fig.3 (c-f). To understand the coherent structure, the normalized two-point correlation function:

$$\widehat{R_{ij}}(\Delta z) = R_{ij}(\Delta z)/R_{ij}(0) = \overline{u_i'(z)u_j'(z+\Delta z)}/\overline{u_i'(z)u_j'(z)}, \qquad (1)$$

in the spanwise direction $\widehat{R_{11}}(\Delta z)$ is discussed. Fig.4 shows some examples of the $\widehat{R_{11}}$ distributions. Although local minima can be seen for all the Re_K cases, their magnitude decreases as Re_K increases. Since the local minimum corresponds to the average spanwise distance between low-speed and neighbouring high-speed regions, the decrease of the magnitude and vanishing oscillations indicate that the streak structure tends to vanish as Re_K increases. From the location of the local minimum, the spanwise spacing of vortex tubes λ_z^{p+} (or λ_z^+ for solid walls) is estimated in Fig.5(a-d). Fig.5(a) compares the solid smooth wall results and published data in the literature (Smith & Metzler, 1983; Kim *et al.*, 1987; Iritani *et al.*, 1985; Tomkins & Adrian, 2003). It is seen that all the data well align on a single curve indicating that the streaks over the solid smooth walls are well organized and their spacing is about 100 of the wall unit under y^+=20 while it gradually increases as the wall normal distance increases. Even though the wall has permeability in Fig.5(b-d), the points of reasonably collapse around the curve under $(y+d)^{p+} \simeq 100$ when the zero-plane displacement d is included in the wall distance. For porous wall flows, the log law defined as the following form Suga *et al.* (2010) is applied.

$$U^+ = \frac{1}{\kappa}\ln\left(\frac{y+d}{h}\right), \qquad (2)$$

where h is the equivalent roughness height. Table 1 lists the values of κ, d and h as well. Indeed, in Fig.5(b-d) plots for #20, #13 and #06 cases are well accord with the line representing the correlation in the solid wall case under $(y+d)^{p+} \simeq 80$, 110 and 80, respectively. Over such regions, which are marked in a hatching zone, plots significantly deviate from the line indicating that the quasi streaky structure tends to be significantly smeared there. To understand the spanwise scale of the structure, the distribution of the spanwise integral length ℓ_{11}^{p+}, which is defined as

$$\ell_{ij} = \frac{1}{2\overline{u_i'(z)u_j'(z)}}\int_{-\infty}^{\infty} R_{ij}(r)dr, \qquad (3)$$

is shown in Fig.6. It is seen that a cluster involving the solid wall case extend up to $(y+d)^{p+} \simeq 300$ while flow motions with much larger scales coexist at $(y+d)^{p+} > 100$.

CONCLUSIONS

At a lower Re_K, low and high speed streaks, which are similar to those of solid-wall turbulence, are observed near the permeable walls. In case of a large Re_K, although some large scale patterns are observed in the velocity field, they are confirmed to be far different from those of the solid wall turbulence structure. It is found that the scales of the structure can be reasonably correlated with the wall normal distance including the zero-plane displacement d of the log-law mean velocity profile. Since there is a correlation between d^{p+} and Re_K (Suga *et al.*, 2010), these phenomena have a correlation with Re_K via d^{p+}. The distribution profiles of the scales

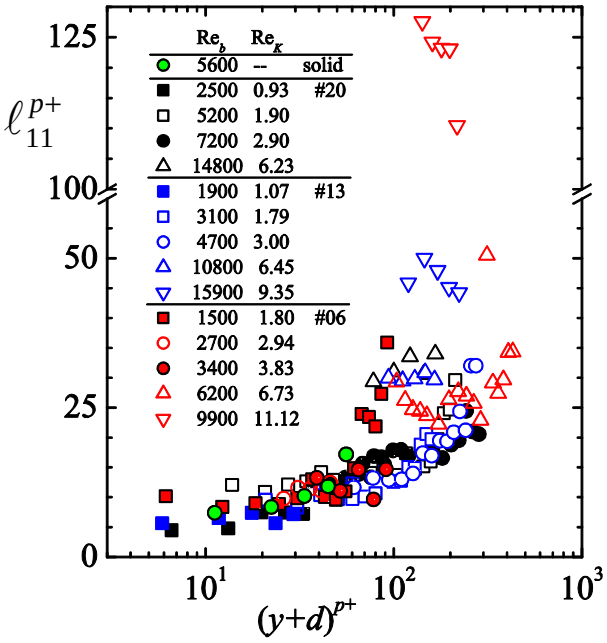

Figure 6. Integral length variations.

indicate that quasi coherent streaks over permeable walls are generated by the wall shear and survive under the transitional range from $(y+d)^{p+} \simeq 100$ while they tend to be disturbed by the K-H instability as the wall normal distance increases. From the region at $(y+d)^{p+} > 100$ flow motions with much larger spanwise length scales start to be dominant. Such flow motions are considered to be transverse roll cells which are generated by the K-H instability and destroy the longitudinal vortex trails. It is considered that fragments of the torn longitudinal vortex tubes surf over the transverse travelling waves. When Re_K is large enough, d^{p+} becomes close to or even surpasses 100 resulting in the loss of the quasi streak structure near the surfaces.

REFERENCES

Breugem, W. P., Boersma, B. J. & Uittenbogaard, R. E. 2006 The influence of wall permeability on turbulent channel flow. *J. Fluid Mech.* **562**, 35–72.

Iritani, Y., Kasagi, N. & Hirata, M. 1985 Heat transfer mechanism and associated turbulence structure in the near-wall region of a turbulent boundary layer. *Turbulent Shear Flows* **4**, 2223–234.

Jiménez, J., Uhlmann, M., Pinelli, A. & Kawahara, G. 2001 Turbulent shear flow over active and passive porous surfaces. *J. Fluid Mech.* **442**, 89–117.

Kim, J., Moin, P. & Moser, R. 1987 Turbulence statistics in fully developed channel flow at low Reynolds number. *J. Fluid Mech.* **177**, 133–166.

Kuwata, Y. & Suga, K. 2016*a* Lattice Boltzmann direct numerical simulation of interface turbulence over porous and rough walls. *Int. J. Heat Fluid Flow* **61**, 145–157.

Kuwata, Y. & Suga, K 2016*b* Transport mechanism of interface turbulence over porous and rough walls. *Flow, Turb. Combust.* **97**, 1071–1093.

Smith, C. R. & Metzler, S. P. 1983 The characteristics of low-speed streaks in the near-wall region of a turbulent boundary layer. *J.*

Fluid Mech. **129**, 27–54.
Suga, K 2016 Understanding and modelling turbulence over and inside porous media. *Flow, Turb. Combust.* **96**, 717–756.
Suga, K., Matsumura, Y., Ashitaka, Y., Tominaga, S. & Kaneda, M. 2010 Effects of wall permeability on turbulence. *Int. J. Heat Fluid Flow* **31**, 974–984.
Suga, K., Mori, M. & Kaneda, M. 2011 Vortex structure of turbulence over permeable walls. *Int. J. Heat Fluid Flow* **32**, 586–595.
Tomkins, C. D. & Adrian, R. J. 2003 Spanwise structure and scale growth in turbulent boundary layers. *J. Fluid Mech.* **490**, 37–74.